Biochimica et Biophysica Acta 1848 (2015) 2932–2941

Contents lists available at ScienceDirect

Biochimica et Biophysica Acta

journal homepage: www.elsevier.com/locate/bbamem

Introducing a fluorescence-based standard to quantify protein partitioning into membranes

Franziska A. Thomas [1], Ilaria Visco [1], Zdeněk Petrášek [2], Fabian Heinemann [3], Petra Schwille *

Max Planck Institute of Biochemistry, Am Klopferspitz 18, D-82152 Martinsried, Germany

ARTICLE INFO

Article history:
Received 27 February 2015
Received in revised form 27 August 2015
Accepted 1 September 2015
Available online 2 September 2015

Keywords:
Partition coefficient
Giant unilamellar vesicles
Fluorescence correlation spectroscopy
Confocal imaging

ABSTRACT

The affinity of peripheral membrane proteins for a lipid bilayer can be described using the partition coefficient (K_P). Although several methods to determine K_P are known, all possess limitations. To address some of these issues, we developed both: a versatile method based on single molecule detection and fluorescence imaging for determining K_P, and a simple measurement standard employing hexahistidine-tagged enhanced green fluorescent protein (eGFP-His_6) and free standing membranes of giant unilamellar vesicles (GUVs) functionalized with NTA(Ni) lipids as binding sites. To ensure intrinsic control, our method features two measurement modes. In the single molecule mode, fluorescence correlation spectroscopy (FCS) is applied to quantify free and membrane associated protein concentrations at equilibrium and calculate K_P. In the imaging mode, confocal fluorescence images of GUVs are recorded and analyzed with semi-automated software to extract protein mean concentrations used to derive K_P. Both modes were compared by determining the affinity of our standard, resulting in equivalent K_P values. As observed in other systems, eGFP-His_6 affinity for membranes containing increasing amounts of NTA(Ni) lipids rises in a stronger-than-linear fashion. We compared our dual approach with a FCS-based assay that uses large unilamellar vesicles (LUVs), which however fails to capture the stronger-than-linear trend for our NTA(Ni)-His_6 standard. Hence, we determined the K_P of the MARCKS effector domain with our FCS approach on GUVs, whose results are consistent with previously published data using LUVs. We finally provide a practical manual on how to measure K_P and understand it in terms of molecules per lipid surface.

1. Introduction

Peripheral membrane proteins are involved in various key cellular processes, e.g. signaling and cell division [1,2]. They can interact with lipid membranes in different ways, for example by lipid modifications or through membrane targeting domains. Besides a direct interaction with a specific lipid molecule (e.g. proteins recognizing phosphoinositol), the membrane binding site of a protein can interact with several outer head groups (e.g. BAR proteins) [3] and/or with the internal hydrocarbon backbone of a lipid area [4–6]. The quantification of membrane affinity of peripheral proteins is challenging but crucial, in order to elucidate the role of lipid composition and the properties of anchoring segments on binding specificity. The partition coefficient (K_P) is an important generic parameter that describes the affinity of a molecular species for lipid bilayers independently from the underlying binding mechanism [7]. For K_P determination in model membrane systems, several methods are known, e.g. fluorescence spectroscopy, equilibrium dialysis, centrifugation or calorimetry. Besides specific advantages, all of them have particular experimental drawbacks, such as changes in lipid and/or protein concentration during the measurement, and low sensitivity. These methods, their advantages and drawbacks were discussed in detail in several review articles [7–11].

Besides the above-mentioned established approaches, few additional microscopy based methods have been proposed to determine the affinity of diverse molecular species for lipid membranes. A quantitative fluorescence recovery after photobleaching (FRAP) approach was applied in live cells to obtain the association and dissociation rate constants k_{on} and k_{off} of intracellular binding-reaction diffusion process [12]. Total internal reflection fluorescence (TIRF) imaging was used to determine the membrane-

Abbreviations: Alexa488, Alexa Fluor 488 carboxylic acid, succinimidyl ester; BSA, albumin from bovine serum; DGS-NTA(Ni), 1,2-di-(9Z-octadecenoyl)-*sn*-glycero-3-[(*N*-(5-amino-1-carboxypentyl)iminodiacetic acid)succinyl] nickel salt; DOPC, 1,2-di-(9Z-octadecenoyl)-*sn*-glycero-3-phosphocholin; eGFP-His_6, hexahistidine-tagged enhanced green fluorescent protein; FCS, fluorescence correlation spectroscopy; GUV, giant unilamellar vesicle; K_d, dissociation constant; k_{off}, dissociation rate constant; k_{on}, association rate constant; K_P, partition coefficient; LUV, large unilamellar vesicle; MARCKS, myristoylated alanine-rich C kinase substrate; NTA, nitrilotriacetic acid; PBS, phosphate buffered saline; POPC, 1-palmitoyl-2-oleoyl-sn-glycero-3-phosphocholine; POPS, 1-palmitoyl-2-oleoyl-sn-glycero-3-phospho-L-serine.

* Corresponding author.
E-mail address: schwille@biochem.mpg.de (P. Schwille).
[1] These authors contributed equally.
[2] Present address: Graz University of Technology, Institute of Biotechnology and Biochemical Engineering, Petersgasse 10-12/I, A-8010 Graz, Austria.
[3] Present address: Roche Diagnostics, Nonnenwald 2, D-82377 Penzberg, Germany.

http://dx.doi.org/10.1016/j.bbamem.2015.09.001
0005-2736/

binding equilibrium constants of a peptide binding to supported lipid bilayers [13]. Finally, confocal imaging of single liposomes was employed to investigate curvature sensing motifs [14]. However, none of these assay-specific microscopy based methods is generally applicable to determine arbitrary K_Ps.

Fluorescence Correlation Spectroscopy (FCS), on the other hand, has been used to determine the K_P of fluorescently labeled peptides to LUVs [15]. In this approach the vesicle-bound and free peptide fractions can be distinguished by their different correlation times. This method offers appealing advantages (e.g. measurement time, extended accessible concentration range) and could be successfully applied for several protein–lipid systems [1,2,16–18] as well as combined with fluorescence spectroscopy to dissect complex partitioning modes [19]. However, potential pitfalls in the data analysis were reported [4–6,20–22]. In our experience, protein-induced vesicle aggregation, as well as variations in protein concentration throughout the measurements, are experimental challenges which may sometimes preclude this approach. A generalized method that still profits from the advantages of using FCS to study membrane dynamics [7–10,23–25], e.g. sensitivity, and at the same time overcomes the above-mentioned limitations is desirable.

Here we describe a new and robust assay, suitable for experimental situations where other methods are not practicable, enabling the direct extraction of quantitative information from the protein systems reconstituted in giant unilamellar vesicles (GUVs). This well-established model membrane system possesses the advantage to be free standing, and thus, protein–lipid interactions are not affected by any support. GUVs have a diameter of 1–100 μm, which easily allows imaging by confocal fluorescence microscopy and permits the simultaneous measurement of both free and bound protein fractions. Also, protein association to GUVs is hardly affected by curvature, the GUV membrane being virtually flat on the nanoscale. Furthermore, GUVs can in principle be produced with any biologically relevant lipid composition and by various methods [12,26].

In our assay, the concentrations of both free and GUV-bound protein are determined at increasing protein concentrations via FCS or confocal fluorescence microscopy. Both approaches provide the advantages to account for potential loss of protein during the measurement (e.g. by protein interaction with the surface of the measurement chamber) as well as for changes in the lipid concentration (e.g. by GUV bursting), and to be sensitive down to nanomolar range. In addition, the partition coefficient can be directly calculated from the measured concentrations, without the need for physical separation of membrane associated and free protein or for change in the optical properties of the protein upon membrane association. For the validation of the method, we chose the well-characterized and easy to reproduce system of hexahistidine-tag (His_6) binding to nickel (Ni) chelated with nitrilotriacetic acid (NTA) [27,28]. We used enhanced green fluorescent protein (eGFP) with a C-terminal His-Tag (eGFP-His_6) as membrane associating protein and GUVs containing 2–5 mol% NTA(Ni) functionalized lipid as membrane model (Fig. 1A). His_6-tagged proteins and NTA(Ni) functionalized lipids are extensively used to reconstitute protein systems in GUVs [29–31]; in particular eGFP-His_6 attached to GUVs containing 20 mol% DGS-NTA(Ni) was recently used as a simplified model system to mimic the membrane bending property of the peripheral proteins Epsin1 and AP180 [32]. To prove the accuracy of our results, we performed the LUV assay [15], whose data analysis was improved to take into account multiple binding of molecules to a single vesicle. Finally, we applied our method to determine the K_P of the effector domain of the natural peripheral MARCKS protein, MARCKS(151–175), and compared our results with published values [15,33].

2. Theory

The affinity of molecular species for membrane surfaces is described by the relation between the concentration $[P_f]$ (mol/m^3) of the unbound species freely diffusing in solution, and the concentration $[P_m]$ (mol/m^3) of the membrane associated fraction. If the total accessible lipid concentration $[L]$ (mol/m^3) is sufficiently large $[L] \gg [P_m]$, so that no saturation of the binding sites under the used experimental condition takes place, and given that the volume and $[L]$ of the system are kept constant, the relation between the two concentrations is linear:

$$[P_m] = \alpha [P_f]. \tag{1}$$

The proportionality constant α is dimensionless and depends on the amount of surface (expressed, for example, by the lipid concentration) and on the characteristics of the interaction between the molecule and the surface. The same relationship holds in case of partitioning between two phases, i.e. aqueous and lipidic, which is described by K_P as follows:

$$K_P = \frac{[P_m]/[L]}{[P_f]/[W]}. \tag{2}$$

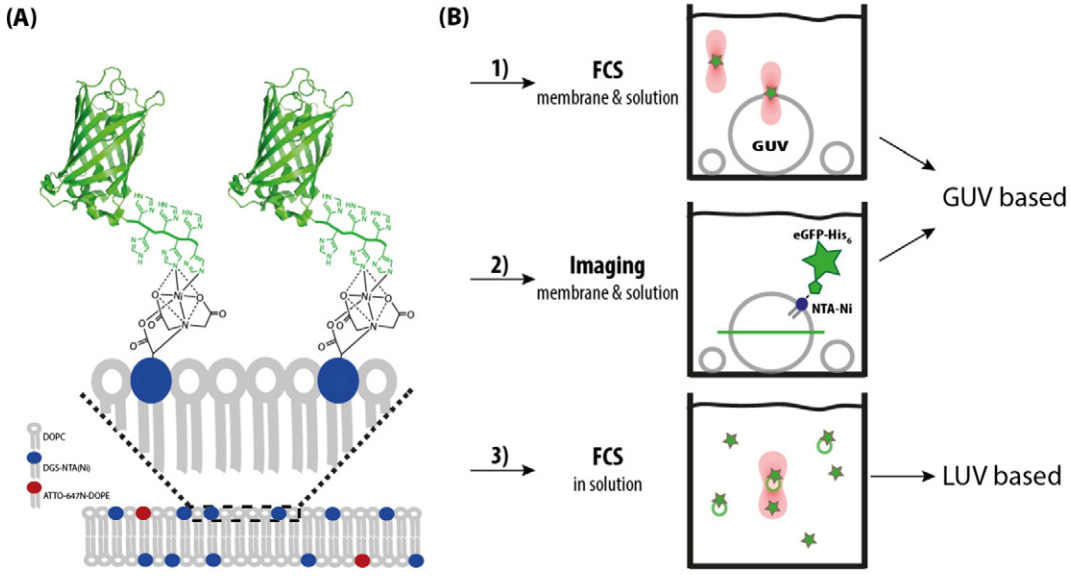

Fig. 1. Schematic representation of (A) the lipid bilayer consisting of DOPC (gray head group), DGS-NTA(Ni) (blue) and the membrane dye ATTO-647N-DOPE (red), illustrating Ni^{2+} coordinating to NTA and to two histidines of His_6-tagged eGFP, and (B) the three applied methods to determine K_P.

A detailed derivation as well as a discussion of the required assumptions can be found in White and colleagues [7]. The water concentration $[W]$ is constant with $[W] = W = 55.5\ M$. $[L]$ is also constant in a given sample and can be expressed by:

$$[L] = \frac{A}{A_L N_A V}. \tag{3}$$

In Eq. (3), A is the total accessible lipid area, A_L is the area per lipid, N_A is the Avogadro's constant and V is the volume of the sample chamber. The importance of Eq. (2) is that it does not make any assumptions about the binding stoichiometry, which is essential since various modes of interaction may play a role in the binding of the same protein to lipid membranes [3].

A convenient way to determine the concentrations in question is to conduct FCS measurements. $[P_f]$ can be quantified performing FCS on free molecules in solution, whereas $[P_m]$ can be obtained by measuring on the membrane of the GUVs. Conveniently, in our assay it is sufficient to measure the surface concentration $[P_{2D}]$ (mol/m^2) on the top pole of a GUV instead of determining $[P_m]$.

$[P_{2D}]$ can be converted to $[P_m]$ by multiplying with the total accessible lipid area A:

$$[P_m] = [P_{2D}]\frac{A}{V}. \tag{4}$$

A rearrangement of Eq. (2) yields in analogy to Eq. (1):

$$[P_m] = \frac{K_P[L]}{W}[P_f]. \tag{5}$$

Combining Eq. (5) with Eqs. (3) and (4) gives the following main equation (A and V cancel out):

$$[P_{2D}] = \frac{K_P}{A_L N_A W}[P_f]. \tag{6}$$

Thus, measuring a set of $[P_{2D}]/[P_f]$ pairs for several concentrations of the binding species leads to a linear behavior with slope:

$$a = \frac{K_P}{A_L N_A W}. \tag{7}$$

When the A_L for the used lipid mixture is known, K_P can be obtained from a, which is not dimensionless (unit of length (m)) but is analog to α. Moreover, $\frac{1}{A_L N_A}$ is the lipid surface concentration $[L_{2D}]$ (mol/m^2), which is constant for a given lipid mixture. Therefore by knowing K_P and $[P_f]$ of the system, one can always calculate the number of molecules per lipid surface, which depends on the combined constant $c = \frac{[L_{2D}]}{W}$ (see Supplementary information, Fig. S1B):

$$[P_{2D}] = c\,K_P[P_f]. \tag{8}$$

Alternatively, both $[P_f]$ and $[P_{2D}]$ can be determined imaging GUVs at their equator. A similar approach was reported for analysis of living cells [15,34]. When a GUV is imaged at its equatorial plane, the fluorescence intensities of its surface and of the surrounding solution are proportional to the concentrations of the membrane bound $[P_m]$ and free molecules $[P_f]$, respectively.

3. Materials and methods

3.1. Materials

1,2-di-(9*Z*-octadecenoyl)-*sn*-glycero-3-phosphocholine (DOPC), 1,2-di-(9*Z*-octadecenoyl)-*sn*-glycero-3-[(*N*-(5-amino-1-carboxypentyl) iminodiacetic acid)succinyl] nickel salt (DGS-NTA(Ni)), 1-palmitoyl-2-oleoyl-*sn*-glycero-3-phosphocholine (POPC), 1-palmitoyl-2-oleoyl-*sn*-glycero-3-phospho-L-serine (POPS) and Avanti Mini-Extruder were purchased from Avanti Polar Lipids (Alabaster, AL). Alexa Fluor 488 carboxylic acid, succinimidyl ester (Alexa488) was obtained from Life Technologies GmbH (Darmstadt, Germany); ATTO-488-NHS, ATTO-655 and ATTO-647N-DOPE from ATTO-Tec (Siegen, Germany). Albumin from bovine serum (BSA) was ordered from Sigma-Aldrich (Schnelldorf, Germany). pGEX-6P-1 vector, Glutathione Sepharose 4 Fast Flow, PreScission Protease and 100 nm polycarbonate membrane were purchased from GE Healthcare (Little Chalfont, United Kingdom).

3.2. eGFP-His$_6$ cloning, expression and purification

eGFP-His$_6$ was cloned into the pGEX-6P-1 vector using the restriction enzymes SalI and NotI and expressed in the *Escherichia coli* strain BL21(DE3). The protein was purified using Glutathione Sepharose 4 Fast Flow according to the manufacturer's instructions, followed by direct cleavage of the glutathione S-transferase tag with PreScission Protease on the column.

3.3. Synthesis and labeling of the MARCKS peptide

The peptide corresponding to the effector domain of the MARCKS protein, MARCKS(151–175) was synthesized with an extra GS linker at the N-terminus using Fmoc-chemistry and labeled at the N-terminus using an ATTO-488-NHS-ester. This is the region of the peptide being most distal to the membrane when the peptide binds and its partition coefficient was shown to not significantly vary from that of radioactively NEM-labeled MARCKS(151–175) (Fig. 1C of Ref [15]). The C-terminus was blocked with an amide group, producing a peptide with 13 positive and zero negative charges. ATTO-488 has one positive and two negative charges at pH 7. The peptide was purified to >90% by preparative RP-HPLC. Purity and identity of the peptide were checked by analytical RP-HPLC and electrospray mass spectrometry. The peptide was stored at −80 °C lyophilized or in water at 1 mg/ml final concentration.

3.4. Preparation of model membranes

3.4.1. Giant unilamellar vesicles

GUVs were prepared by the electroformation method [35]. Briefly, 5 μl of the corresponding lipid mixture (2 mg/ml in chloroform) was spread and dried onto two Pt-wires and put into a homemade teflon chamber filled with 350 μl of 300 mM sucrose. An AC electric field of 2 V was applied to the chamber at a frequency of 10 Hz for 1 h, followed by 2 Hz for 0.5 h. Experiments were carried out in 120 μl MatriCal 384-multiwell plates (Matrical biosciences — now Brooks Life Science Systems, Spokane, USA). For the NTA(Ni)-His$_6$-system, DOPC and 2, 3, 4 or 5 mol% DGS-NTA(Ni) were mixed and labeled with 0.05 mol% ATTO-647N-DOPE. The wells were passivated with 2 mg/ml BSA for at least 30 min and washed two times with phosphate buffered saline (PBS — 137 mM NaCl, 2.7 mM KCl, 4.3 mM Na_2HPO_4, 1.4 mM KH_2PO_4, pH 7.4). The obtained GUVs were diluted 1:50 in sucrose solution and then 1:3 in PBS buffer. Into a well containing 80 μl of PBS buffer 20 μl of the GUV dilution in PBS was added. In case of the MARCKS peptide, GUVs contained 5, 12.5 or 20 mol% POPS in POPC and 0.01 mol% ATTO-647N-DOPE as a lipid dye. The wells were passivated with 0.53 mg/ml POPC small unilamellar vesicles over night and washed ten times with working buffer (10 mM HEPES pH 7, 100 mM NaCl). The obtained GUVs were diluted 1:10 in sucrose and 20 μl of the dilution was transferred into a well, containing 80 μl of working buffer.

3.4.2. Large unilamellar vesicles

DOPC and 2, 3, 4 or 5 mol% DGS-NTA(Ni) were mixed in chloroform. After solvent evaporation, the lipid film was rehydrated in PBS buffer at 10 mg/ml lipid concentration and resuspended by vortexing. The

vesicle suspension was then subjected to eight freeze-thaw cycles and extruded 21 times through a polycarbonate membrane. LUV size and monodispersity were checked via dynamic light scattering (DynaPro NanoStar™, Wyatt Technology Corporation, Santa Barbara, CA) and lipid concentration in LUV preparations was determined by phosphorous assay [36] after extensive dialysis in the presence of non-solubilizing concentrations of TritonX-100. The measured LUV size and lipid concentration were used to calculate the accessible LUV concentration [*LUV*] [37] and the number of lipids contained in a LUV N_{LUV}. Experiments were carried out in homemade observation chambers obtained by gluing cut PCR tubes on a #1.5 coverslip (Gerhard Menzel GmbH, Thermo Fisher Scientific, Braunschweig, Germany) with a UV optical adhesive (NOA63, Norland Products Inc., Cranbury, NJ). The wells were passivated with a 2 mg/ml BSA solution for at least 30 min and rinsed with water and PBS. LUVs were 10-fold serially diluted in PBS, incubated at the desired final concentrations with 50 nM eGFP-His_6 and transferred in the homemade observation chambers.

3.5. Fluorescence measurements

3.5.1. Optical setup

All measurements were carried out on a commercial laser scanning microscope LSM 780 with a ConfoCor 3 unit (Zeiss, Jena, Germany) using a water immersion objective (C-Apochromat, 40×/1.2 W UV–VIS–IR, Zeiss, Jena, Germany). A λ/4 plate was implemented into the light pass to excite by circularly polarized light and ensure uniform excitation. Samples were excited by 488 nm line of an Ar-ion-laser (fluorescence detection range: FCS-GUV 505–575 nm, FCS-LUV 505–610 nm, imaging 491–569 nm) and by 633 nm line of a He–Ne laser (fluorescence detection range: FCS-GUV LP655 nm, imaging 638–759 nm). Laser powers were kept very low in order to avoid laser power related problems such as in focus bleaching or saturation [38]. The experiments were carried out at 26.0 ± 0.5 °C, measured in solution with a digital electrode thermometer Voltcraft K202 (Conrad Electronic, Hirschau, Germany). The setup was calibrated using aqueous solutions (~50 nM) of freely diffusing Alexa488 ($D = 435\ \mu m^2/s$ 22.5 ± 0.5 °C [39]) and in case of the GUV assay free ATTO-655 ($D = 426\ \mu m^2/s$ 25 °C [40]) in a 1:1 ratio. The objective correction collar and the pinhole position (d = 35 or 40 μm for the 488 line alone or both laser lines, respectively) were adjusted to maximize the fluorescence intensity. Correction of diffusion coefficients to the measurement temperature [38], allowed us to determine the parameters of the detection volume: the focal waist $w_0 = \sqrt{4D\tau_D}$, the focal volume $V_{FCS} = \pi^{3/2} S {w_0}^3$ with the structural parameter S and the focal area $A_{FCS} = \pi {w_0}^2$ after a weighted fit of the auto-correlation curves (Alexa488: 3D + T diffusion model, ATTO-655: 3D diffusion model without triplet correction).

3.5.2. GUV data acquisition and analysis by FCS

Per sample a minimum of eight GUVs were selected and measured by point FCS at least at five increasing concentrations of protein. The background signals in solution and on the membrane were recorded before protein addition, since especially at low protein concentrations, and therefore at low fluorescence intensities, the fluorescence background will affect the particle number obtained from the fit. We used PyCorrFit 0.7.4 [41] to analyze the auto-correlation curves and Origin 9.0G for fitting.

Protocol to measure K_P *by Fluorescence Correlation Spectroscopy in GUVs*

1. Determine the number of particles N_f freely diffusing and their diffusion time τ_D from a point-FCS measurement of ten times 30 s in solution. Use a non-weighted fit of the fluorescence auto-correlation curves with the suitable FCS model function for 3D + T diffusion to obtain the number of free particles N_f' in the observation volume and a weighted fit to get τ_D. Remove the after pulsing (2 μs), fix τ_T to 0.02 ms and S to the value obtained in the calibration measurement. Correct N_f' for the background [42] to get N_f
2. Calculate $[P_f]$ from N_f as follows:

$$[P_f] = \frac{N_f}{V_{FCS} N_A} \tag{9}$$

3. Determine the number of particles N_{2D} bound to a GUV from a point-FCS measurement of five times 30 s at the top pole of the GUV [38]. Use a combined 2D–3D fit, since both, freely diffusing molecules and membrane bound molecules will be present in the detection volume, fixing τ_D to the value obtained in solution. From the fit, the fraction F of free protein in solution and the total particle number N_{2D3D}' in the focal volume will be obtained. Since τ_D is obtained by an external measurement and differs by at least an order of magnitude from the 2D diffusion time in the membrane, F is robustly determined under particle counts recommended for FCS [43]. After correcting N_{2D3D}' for the background, the particle number N_{2D} in the FCS observation area A_{FCS} can be calculated:

$$N_{2D} = (1-F) N_{2D3D} \tag{10}$$

4. Use N_{2D} to calculate $[P_{2D}]$:

$$[P_{2D}] = \frac{N_{2D}}{A_{FCS} N_A} \tag{11}$$

5. Plot $[P_f]$ against $[P_{2D}]$ and fit the graph with a x/y-weighted linear model to obtain the slope a.
6. Knowing A_L, calculate K_P from the slope a

$$K_P = a\, A_L\, N_A\, W. \tag{12}$$

3.5.3. GUV data acquisition and analysis by Image Analysis

Images of the same GUVs as in the GUV–FCS approach were taken at approximately their equator using avalanche photodiodes as detectors in the confocal microscope. In order to extract the membrane bound and free fluorescence intensities I_{2D} and I_f from the confocal GUV images, a semi-automated software was developed (Fig. 2).

Each I_{2D} was correlated to the corresponding concentration $[P_{2D}]$ determined by FCS in Origin 9.0G and analyzed by a linear fit passing through the origin of the graph. Analogously the averaged mean intensities in solution I_f were related to $[P_f]$.

Protocol to calibrate the *Image Analysis in GUVs*

1. Determine $[P_{2D}]$ and $[P_f]$ of several GUVs by FCS as described in the "Protocol to measure K_P *by Fluorescence Correlation Spectroscopy in GUVs*" or by any other method of choice.
2. Take images of the same GUVs at approximately their equator using a photon counting detector (i.e. avalanche photodiodes).
3. Extract the surface and free fluorescence intensities I_{2D} and I_f from the confocal GUV images, using for example our semi-automated software (the Matlab source is available upon request). For each GUV to analyze, the user enters approximate coordinates of the GUV center and an approximate radius. The software then determines the precise GUV center position and approximates the circumference of the GUV cross-section by a smooth closed curve. This allows the extraction of the radial intensity profile of the GUV. From the intensity profile the surface fluorescence intensity I_{2D} and the solution fluorescence intensity I_f are determined. Additionally, it is possible to exclude a range of angles (`a wedge') from the analysis, which is useful, for example, when two GUVs are in contact. The ring region outside the GUV (an interval of radial distance in the

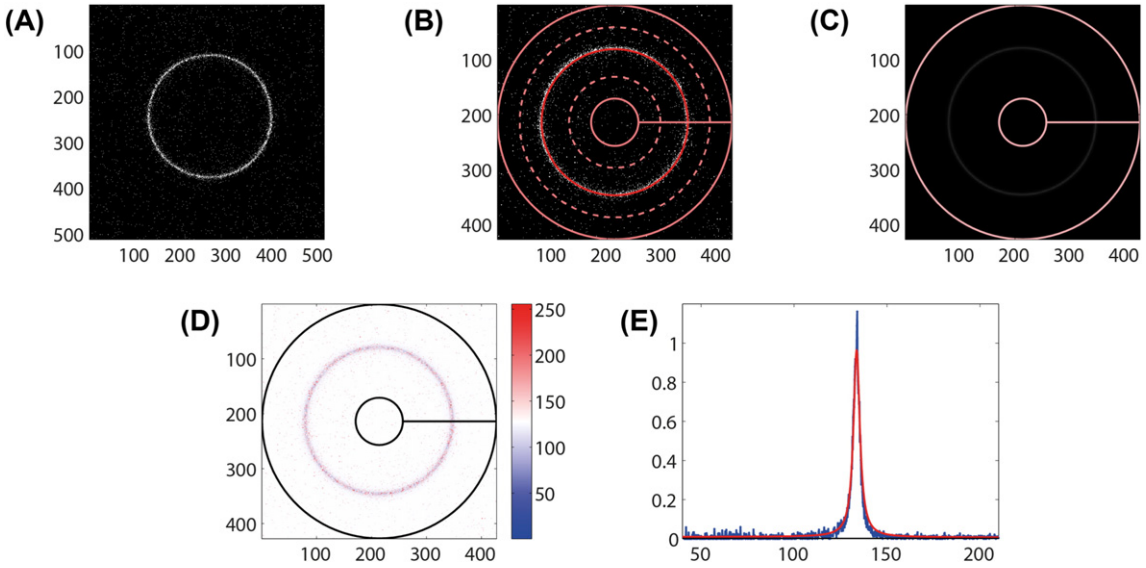

Fig. 2. GUV image analysis. (A) GUV with rescaled intensity, (B) the ring area between the two dashed lines is used to determine the surface concentration (bound fraction, I_{2D}), the mean intensity inside the GUV is calculated from the innermost ring area, and the intensity outside the GUV from the outermost ring, (C) fit of the GUV shape and intensity within the selected area, (D) fit residuals, (E) the experimental (blue) and fitted (red) radial profile of GUV. Image scale: (A)–(D) x- and y-axis in pixel, (E) x-axis in pixel and y-axis in average photons per pixel.

radial intensity profile) from which I_{2D} is determined is typically constant for all GUVs and need not be adjusted individually.
4. If necessary subtract the background of the GUVs before protein addition from the mean intensities.
5. Plot I_{2D} and I_f intensities against $[P_{2D}]$ and $[P_f]$ concentrations determined by FCS or by another method, respectively and fit each graph with a linear model passing through the origin of the graph to obtain the two proportionality constants b_{2D} and b_f.

Protocol to measure K_P *by Image Analysis in GUVs*

1. Repeat steps 2–4 of the "Protocol to calibrate the *Image Analysis in GUVs*" for several GUVs
2. Calculate $[P_{2D}] = b_{2D} I_{2D}$ and $[P_f] = b_f I_f$
3. Repeat steps 5–6 of the "Protocol to measure K_P *by Fluorescence Correlation Spectroscopy in GUVs*"

3.5.4. LUV data acquisition and analysis

For each DOPC:DGS-NTA(Ni) molar ratio, at least three independent samples were investigated at eight different LUV concentrations (1 μM–10 mM). For each LUV concentration, point-FCS was measured four sequential times and for each of them ten independent fluorescence intensity tracks of 10 s each were acquired. The FCS auto-correlation curves were calculated using the Zeiss ZEN 2011 Black edition software and analyzed using PyCorrFit 0.8.1 [41] and SigmaPlot 12.3 (Systat Software, Inc., San Jose, CA).

Protocol to measure K_P *by Fluorescence Correlation Spectroscopy in LUVs*

1. Determine the protein concentration $[P]$ and the diffusion time of the free protein τ_f from the point-FCS measurements of a solution of the protein in the absence of LUVs. Use a non-weighted 3D + T-fit to get the number of particles N, and a weighted fit to get the τ_f, fixing S to the value obtained in the calibration measurement. $[P]$ can be calculated from N as follows:

$$[P] = \frac{N}{V_{FCS} N_A} \tag{13}$$

2. Determine the total number of particles N_{f+m} (free + vesicle bound protein) from the point-FCS measurements of a solution of the protein in the presence of different concentrations of LUVs. Use a non-weighted two components 3D + T-fit, fixing S and τ_f to the values obtained in the calibration measurements and in the absence of LUVs, respectively.
3. Calculate an average $G(0)$ value for each LUV concentration of a sample and normalize by the $G(0)$ value in the absence of LUV using $G'(0) = \frac{N}{N_{f+m}}$.
4. To obtain K_d, plot the $G'(0)$ values against the accessible LUV concentration and fit, fixing $[P]$ to the value obtained in the absence of LUVs, with the following equation:

$$G'(0) = 1 + \frac{[P][LUV]}{(K_d + [LUV])^2} \tag{14}$$

5. If needed convert the obtained K_ds to K_P:

$$K_P = \frac{W N_{\mathrm{LUV}}}{K_d} \tag{15}$$

N_{LUV} is the number of lipids contained in a LUV.

4. Results and discussion

4.1. GUV based assay by FCS

For the calculation of the partition coefficient K_P, it is essential to precisely determine the amount of both freely diffusing and DGS-NTA(Ni)-coordinated eGFP-His_6. In order to quantify both concentrations, we conducted point-FCS in solution and on the top pole of several GUVs per probe.

Before measurement of each sample, the system was carefully calibrated with Alexa488 to calculate the focal waist w_0, V_{FCS} and A_{FCS}. The latter two need to be determined precisely, since an error of their values propagates in the calculation of all protein concentrations. Here it is of importance to rely on dyes with a well known diffusion coefficient and correct for its temperature dependency [38,43]. The average values obtained of all measurements are $w_0 = 218.0 \pm 6.0$ nm (mean ± s.e.m., n = 19), $V_{FCS} = 3.98 \pm 0.36 \cdot 10^{-19} m^3$ (mean ± s.e.m., n = 19) and $A_{FCS} = 1.49 \pm 0.08 \cdot 10^{-13} m^2$ (mean ± s.e.m., n = 19). As

an additional control, the red channel was calibrated as well using ATTO-655 having a focal waist $w_0 = 246.2 \pm 4.6$ nm (mean ± s.e.m., n = 19) due to greater diffraction.

Thereafter, an overall image of the well in which the experiment was carried out was taken by a tile scan. Sequentially, more GFP-His_6 was added into the chamber and incubated until equilibrium was reached. For each protein concentration, the auto-correlation functions of both the free and bound protein signals were recorded. The system was very stable over time and therefore for each of the increasing amounts of protein exactly the same GUVs could be surveyed. Additionally, the ATTO-647 N-DOPE signal was taken simultaneously to control the state of the membrane upon protein binding. Protein and lipid average diffusion coefficients of this system were reported elsewhere [44]. Fluorescent lipids in traces are commonly used in the presence of His_6-tagged proteins reconstituted in GUVs [30,45] and are not reported to interfere with their binding to DGS-NTA(Ni) lipids. Among several fluorescent lipids available, ATTO-647N-DOPE was chosen because it has low triplet formation and it is spectrally well separated from eGFP (product specification, www.atto-tec.com). In case the fluorescence time traces showed a strange behavior, the curves of both channels were rejected. At higher concentrations of DGS-NTA(Ni), the laser power of the 488 laser line needed to be reduced to avoid detector saturation, which does not significantly affect the concentration measurement by FCS, but has to be considered for the image analysis by using an appropriate calibration curve.

The successive auto-correlation curves taken in solution were fitted using 3D function in PyCorrFit [41] and Eq. (13) to get $[P_f]$. The average diffusion time of eGFP-His_6 in solution is $\tau_D = 1.23 \pm 0.02 \cdot 10^{-4}$s (mean ± combined s.e.m., n = 890), from which the average diffusion coefficient can be calculated. The obtained value of $D = 103 \pm 6\,\mu m^2/s$ (mean ± combined s.e.m.; 26.0 ± 0.5 °C) is in agreement with previous measurement [39].

Analogously, the corresponding auto-correlation functions taken on membrane were fitted using 2D-3D fit function to get the average number of particles, which was used to calculate the bound protein concentration $[P_{2D}]$ according to Eqs. (10) and (11).

In Fig. 3 a typical graph of a measurement is shown with the obtained $[P_f]$ and $[P_{2D}]$ plotted against each other. The relatively high error bars for $[P_{2D}]$ are possibly a result of an — to some extent unavoidable — uneven distribution of the DGS-NTA(Ni) among the GUVs in the sample [46]. However, this emphasizes the need to minimize sample inhomogeneity in order to reduce the experimental error. As assumed in the theory, the linear relation between $[P_f]$ and $[P_{2D}]$ confirms that no saturation of the binding sites takes place.

To calculate the partition coefficient K_P for a particular percentage of DGS-NTA(Ni), the slope a and A_L for the given system are required. For our calculations, we used 72.4 Å^2 for DOPC [47] and for DGS-NTA(Ni) an A_L of 60.0 Å^2 [48]. We estimated A_L by linear interpolation of the two values, yielding 72.2 Å^2, 72.0 Å^2, 71.9 Å^2 and 71.8 Å^2 for the molar ratios 2%, 3%, 4% and 5% of DGS-NTA(Ni) in the lipid mixture with DOPC.

Fitting all data points of at least three independent measurements results in a slope a for the percentage of DGS-NTA(Ni), out of which the K_P was calculated using Eq. (12). In Table 1 and Fig. 4 the results of our investigations are summarized. Identical values are gained by averaging the individual measurements and using a combined standard deviation, small variations are due to differences in sample size.

Our results clearly show that eGFP-His_6 binds stronger to the membrane of the GUVs with increasing amounts of DGS-NTA(Ni) in the lipid mixtures. So far no K_P was reported for eGFP-His_6 coordinated to DGS-NTA(Ni), but a direct comparison to the published K_d values is feasible [44].

4.2. GUV based assay by image analysis

Besides the FCS on the top pole of the GUVs as described in the previous paragraph, we imaged the equator of the same GUVs. In Fig. 2A-E the typical output of the analysis of a GUV image is shown. It is necessary to correlate only once the mean intensity obtained by image analysis to the concentration determined by another method, in our case FCS.

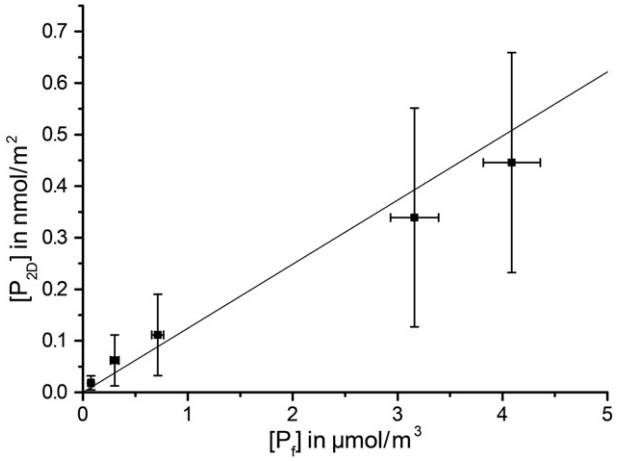

Fig. 3. eGFP-His_6 concentrations determined by GUV–FCS assay. $[P_{2D}]$ plotted vs. $[P_f]$ for an individual sample of 2% DGS-NTA(Ni). Error bars represent the standard deviation. The ratio of $[P_{2D}]/[P_f]$ stays constant with increasing protein concentration. No saturation occurs.

In Fig. 5 example plots of all pairs of data points for 2% DGS-NTA(Ni) for $[P_{2D}]$ and $[P_f]$ and their corresponding mean intensities I_{2D} and I_f are shown. The slope b obtained by a linear fit does not depend on the amount of DGS-NTA(Ni), neither for the free nor for the bound eGFP-His_6. Hence, the combined mean slope b_{2D} and the mean intensity of the membrane bound eGFP-His_6 for a particular laser power can be used to calculate the concentration of membrane bound protein $[P_{2D}]$. Similarly, $[P_f]$ can be determined using b_f and the mean intensity of the free eGFP-His_6. Therewith K_P was calculated as described for the FCS approach. The results (Table 1) are equivalent to those obtained by the FCS approach.

4.3. LUV based assay by FCS

To validate our assay, we measured the affinity of eGFP-His_6 for DGS-NTA(Ni)-containing vesicles with an alternative LUV based assay [15]. Here, the calculation of K_p relies on the precise measurement of the total amount N_{f+m} of eGFP-His_6 particles in solution; eGFP-His_6 particles can be both freely diffusing or coordinated to the DGS-NTA(Ni) embedded in the vesicles. In order to quantify the total amount of eGFP-His_6 particles, we performed one-color point-FCS in solution at different time points per probe.

Before measuring each sample, the system was calibrated using Alexa488 as described for the GUV based assay. The average values obtained for all measurements are $w_0 = 205.7 \pm 1.6$ nm (mean ± s.e.m., n = 15) and $V_{FCS} = 2.98 \pm 0.10 \cdot 10^{-19} m^3$ (mean ± s.e.m., n = 15).

In contrast to the GUV based assay, the amount of eGFP-His_6 was kept constant and equilibrated with different LUV concentrations. In particular, eGFP-His_6 was gently mixed with the vesicles and subsequently

Table 1
Comparison of K_Ps. Calculated partition coefficients by fitting all data points for increasing amounts of DGS-NTA(Ni) via the GUV and LUV methods (mean ± combined s.e.m.).

DGS-NTA(Ni)	A_L	K_P GUV–FCS	K_P GUV-imaging	K_P LUV–FCS[a]
2%	72.2 Å^2	$2.54 \pm 0.27 \cdot 10^6$	$2.79 \pm 0.10 \cdot 10^6$	$1.33 \pm 0.23 \cdot 10^6$
3%	72.0 Å^2	$4.34 \pm 0.88 \cdot 10^6$	$4.56 \pm 0.34 \cdot 10^6$	$1.74 \pm 0.10 \cdot 10^6$
4%	71.9 Å^2	$1.54 \pm 0.11 \cdot 10^7$	$1.35 \pm 0.05 \cdot 10^7$	$1.90 \pm 0.18 \cdot 10^6$
5%	71.8 Å^2	$4.82 \pm 1.13 \cdot 10^7$	$3.55 \pm 0.14 \cdot 10^7$	$2.21 \pm 0.22 \cdot 10^6$

[a] The differences at higher DGS-NTA(Ni) molar fraction (3–5 mol%) between GUV- and LUV- assay are due to protein-induced LUV aggregation (see Section 4.5 and Fig. S2).

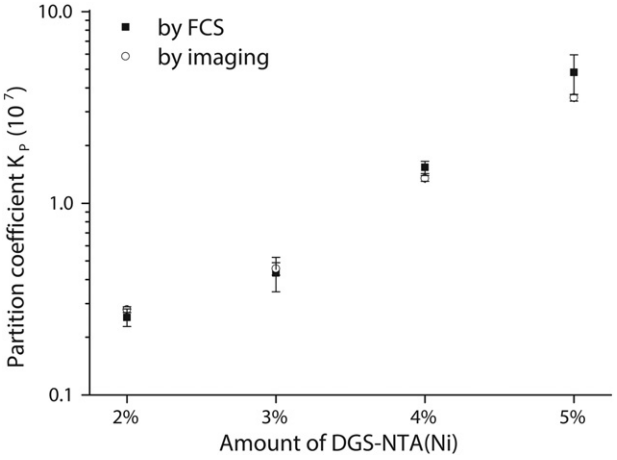

Fig. 4. K_p determined by GUV assay. Graphic presentation of partition coefficient K_P obtained by fitting of all data points from FCS analysis (filled squares) and image analysis (circles) for a certain concentration of DGS-NTA(Ni). Error bars represent the combined standard error of mean. K_P shows a stronger-than-linear behavior. Results of LUV–FCS are excluded, since they are presumably distorted by LUV aggregation (see Section 4.5 and Fig. S2).

transferred to the observation chamber to assure that the protein would be evenly distributed all over the chamber and the binding equilibrium would be reached faster. Moreover, to minimize changes in the total volume of the sample, each LUV concentration was sequentially probed in a separate chamber; FCS measurements were performed always at the same distance from the bottom of the chamber to avoid any surface related dependencies [49,50]. In these conditions background correction was not necessary, since the eGFP signal is stable and significantly higher than the background level.

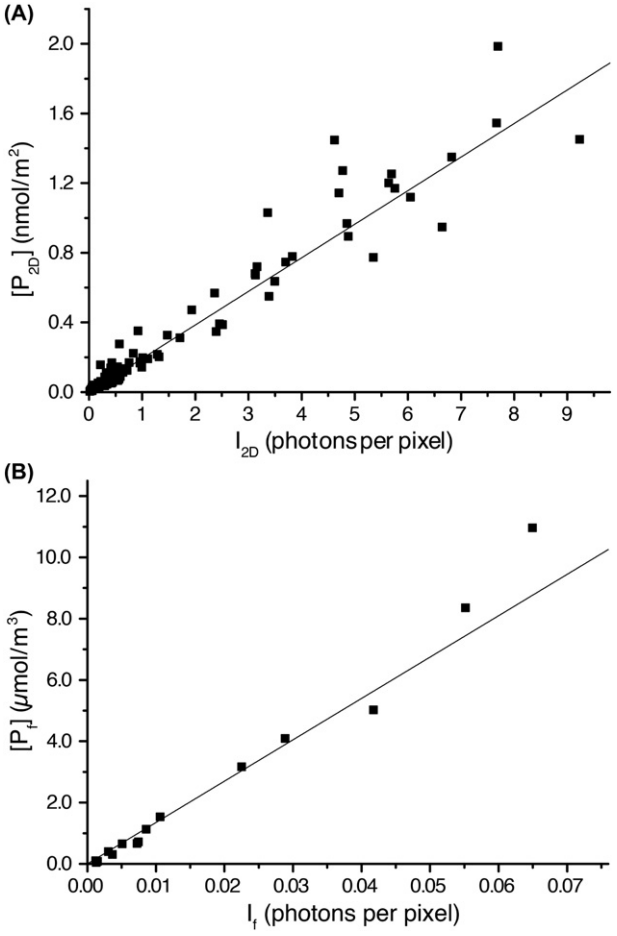

Fig. 5. Calibration curve for GUV-image analysis. Mean intensity obtained by image analysis plotted against the concentration determined by FCS (A) on the membrane and (B) in solution of all data points of 2% DGS-NTA(Ni). Both curves show a linear behavior and the slopes b_{2D} and b_f are used to calculate the protein concentration directly from the mean intensities.

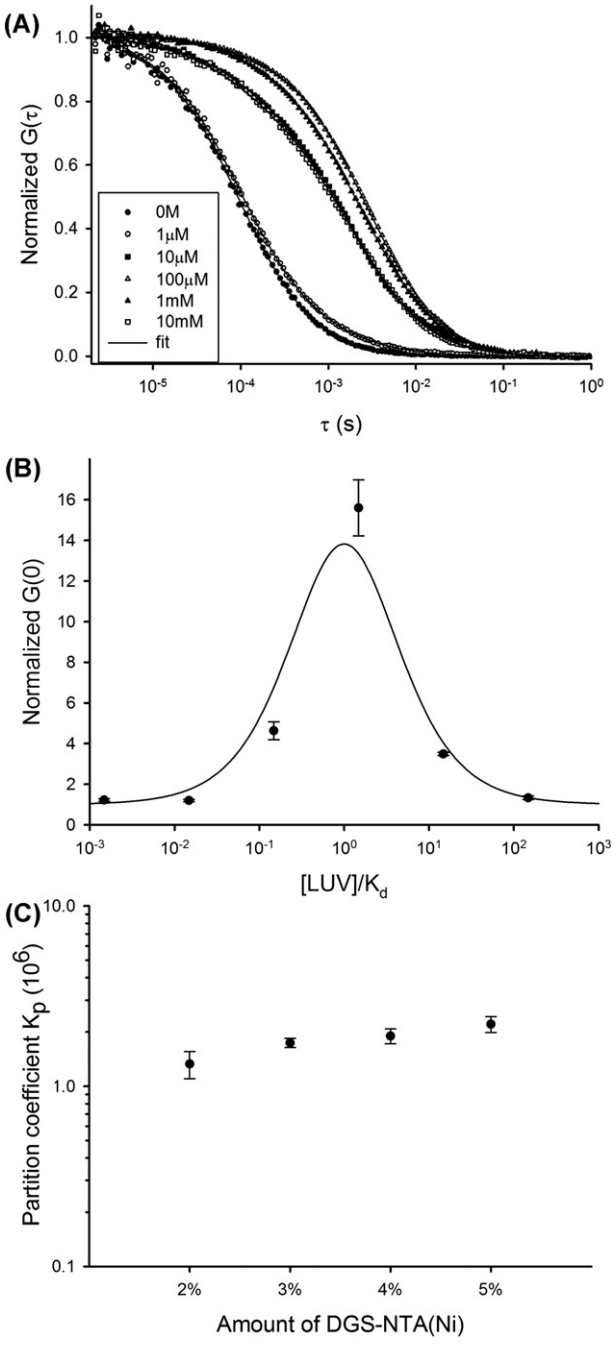

Fig. 6. LUV–FCS assay. (A) auto-correlation curves obtained in solution for eGFP-His_6 in the absence (0 M) and presence of increasing amounts of LUVs (1 μM, 10 μM, 100 μM, 1 mM, and 10 mM). Solid lines are the best fit of the data with a single (0 M) or two-components (all other curves) 3D diffusion model, (B) Normalized G(0) data points for a single 2% DGS-NTA(Ni) sample are plotted against the ratio [LUV]/K_d. The solid line is the best fit of the data using Eq. (14), (C) Graphic presentation of partition coefficients K_Ps obtained from K_d (Eq. (15)).

The auto-correlation functions of eGFP-His_6 in solution were recorded in the absence of LUVs and fitted using a 3D + T function to obtain [*P*] and the average diffusion time $\tau_f = 0.96 \pm 0.05 \cdot 10^{-4}$s ($D = 110 \pm 7$ μm^2/s; mean ± combined s.e.m.; 26.0 ± 0.5 °C), respectively. The

auto-correlation functions of eGFP-His_6 in the presence of increasing amounts of LUVs were fitted with a two component 3D + T function, keeping τ_f constant, to get the total number of eGFP-His_6 particles N_{f+m}. A fraction of the acquired auto-correlation functions were affected by eGFP-His_6-induced LUV aggregation [22], as reveled by their distorted form (Supplementary information, Fig. S2). These curves were not included in the analysis. As expected, the eGFP-His_6 diffusion time increases upon binding to LUVs (Fig. 6A), as far as the vesicles are significantly larger than the protein. At the same time, N_{f+m} decreases, meaning that more than a single eGFP-His_6 molecule bind each LUV. At higher LUV concentration N_{f+m} starts increasing again to reach the original value of freely diffusing eGFP-His_6, suggesting that upon further addition of LUVs the eGFP-His_6 molecules redistribute so that the probability of more than one eGFP-His_6 binding to one LUV is negligible (Fig. 6B).

From the total number of eGFP-His_6 particle values measured in at least three independent samples (e.g. Fig. 6B), a G(0) was calculated for each LUV concentration and normalized to the G(0) in the absence of LUVs. The data points were then fitted with Eq. (14) to obtain K_d for a particular percentage of DGS-NTA(Ni) in the lipid mixture. The protein and accessible lipid concentration values used for the fit were determined experimentally. The total protein concentrations were calculated from the number of eGFP-His_6 particles measured by FCS in the absence of LUVs, whereas the accessible lipid concentrations were obtained measuring both the total lipid concentrations and vesicle sizes (see Materials and methods section for details). The dissociation constant K_d was finally transformed into K_P values for comparison applying Eq. (15) (Fig. 6C).

4.4. K_P of the MARCKS peptide determined by the GUV–FCS assay

In order to prove the applicability of our method to biological peripheral proteins, the molar partition coefficients K_P of the peptide corresponding to the effector domain of the MARCKS protein, MARCKS(151–175) was determined with the GUV–FCS approach.

Before measuring each sample, the system was calibrated using Alexa488 as described for the NTA(Ni)-His_6 system. The average values obtained of all measurements are $w_0 = 219.0 \pm 7.0$ nm (mean ± s.e.m., n = 13), $V_{FCS} = 3.43 \pm 0.39 \cdot 10^{-19}\,m^3$ (mean ± s.e.m., n = 13) and $A_{FCS} = 1.53 \pm 0.11 \cdot 10^{-13}\,m^2$ (mean ± s.e.m., n = 13). MARCKS peptide was added in several wells at different concentrations. The auto-correlation curves taken in the absence of GUVs were fitted using a 3D model function in PyCorrFit [41] to get the average diffusion time of the MARCKS peptide in solution. The obtained value of $\tau_D = 64.3 \pm 4.1 \cdot 10^{-6}$ s (mean ± combined s.d., n = 23) is in agreement with previously reported results [15]. The same amount of GUVs was next added in each well and incubated until equilibrium was reached. To easily identify the GUVs, an overall image of the well was taken by a tile scan. For each GUV, the auto-correlation functions of both the free and bound protein signal were recorded and analyzed as described for the NTA(Ni)-His_6 system. For these calculations, we used an A_L of 68.3 Å^2 for POPC [51] and of 62.7 Å^2 for POPS [52]. We estimated A_L by linear interpolation of the two values, yielding 68.0 Å^2, 67.6 Å^2 and 67.2 Å^2 for the molar ratios of 5%, 12.5% and 20% POPS in the lipid mixture with POPC. K_P values for each percentage of POPS were calculated fitting at least three independent data sets (Fig. 7).

The obtained results are in line with the values reported by Arbuzova et al. [33] using sucrose loaded vesicles and radioactively labeled peptide and by Rusu et al. [15] using the LUV–FCS method.

4.5. Comparison of methods

In both GUV based approaches, GFP-His_6 shows a strong affinity for the membrane, which derives from the nature of the His-tag NTA(Ni) chelation, which is not purely electrostatic, but involves the formation of a more stable coordination bond. GFP-His_6 affinity for the membrane

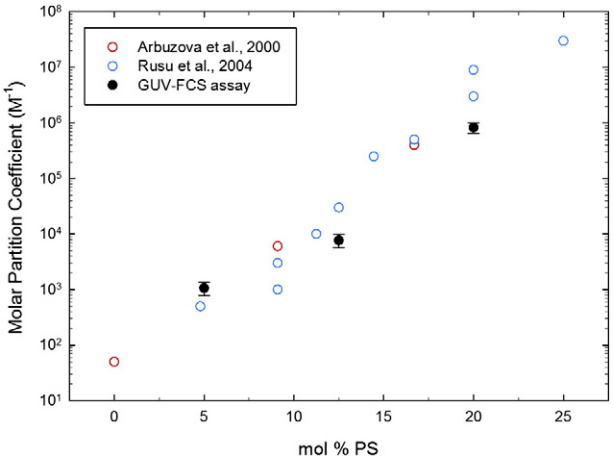

Fig. 7. MARCKS peptide measured with the GUV–FCS assay (black closed circles) are in line with the values reported by Arbuzova et al. 2000 using sucrose loaded vesicles and radioactively labeled peptides ([33], red open circles) and by Rusu et al. 2004 using the LUV–FCS method ([15], estimated from Fig. 4 of the reference, blue open circles). Error bars represent standard deviations.

increases non-linearly with higher contents of nickel–lipid in the bilayer, as observed for the MARCKS peptide and in other systems [15,22]. B. Ernst and colleagues analyzed the binding/dissociation of different oligo-His-tags to NTA(Ni) [27] and showed that for high surface densities of NTA(Ni) a rebinding effect plays an important role. Under these conditions eGFP-His_6 might interact with several DGS-NTA(Ni) [53,54]. Hence, for higher DGS-NTA(Ni) contents, the equilibrium is strongly shifted to the bound fraction, resulting in a stronger-than-linear increase of K_P. The LUV assay failed to capture this trend.

The results obtained for GUVs and LUVs containing equal amounts of DGS-NTA(Ni) are shown in Table 1. At low DGS-NTA(Ni) molar fraction (2 mol%), the K_Ps measured with both GUV- and LUV-methods differ by a factor of two (GUV-method: $2.51 \pm 0.19 \cdot 10^6$; LUV-method: $1.33 \pm 0.23 \cdot 10^6$), whereas at higher DGS-NTA(Ni) molar fraction (3–5 mol%) they differ up to one order of magnitude. We assume that the observed differences are an artifact of the LUV–FCS method, due to LUV aggregation, which increases with lower lipid/protein ratios [22] and higher DGS-NTA(Ni) molar fractions (see Supplementary information, Fig. S2). It was shown that vesicles containing DGS-NTA(Ni) can aggregate after addition of synthetic peptides with poly-histidine residues and that the aggregation is dependent on the DGS-NTA(Ni) amount present in the vesicles [55]. Therefore, the measured total number of eGFP-His_6 particles in solution N_{f+m}, which is critical for deriving K_P, does not only depend on the lipid binding properties of the protein, but it is influenced by the amount of protein and vesicles sequestered in the aggregated form. In contrast to LUVs, no lipid or protein aggregation takes place in GUVs upon eGFP-His_6 binding. When the ligand does not induce LUV aggregation as in case of the effector domain of the MARCKS protein, MARCKS(151–175) [15], the K_P values obtained by the GUV- and the LUV–FCS approach are comparable (Fig. 7). On the other hand, in both GUVs based approaches, the protein and accessible lipid concentrations need to be carefully chosen in order to measure precisely in solution and at the membrane. For high binding affinities, the concentration at the membrane could be already high while there are no detectable amounts of proteins in solution, which set the upper range of accessible K_P to approximately 10^8. Interestingly the GUV–FCS approach appears to be less precise than the GUV-imaging one, as shown by the relatively high error bars for [P_{2D}]. This can be explained taking into account how the free protein concentration is measured in the FCS and imaging approaches, only once for the whole chamber and close by each GUV, respectively. Technically it should be enough to measure the free protein concentration once, but more precise values can be determined with the GUV-imaging approach. The precision of

the GUV–FCS assay could be improved measuring FCS in solution next to each GUV (Fig. 7), but this doubled the measuring time.

Importantly, both GUV based approaches possess the advantage over the LUV method of directly visualizing the binding event and thus of being able to correct anomalies in the sample. Having an overview of the whole chamber, it is possible to select and continuously measure the same GUVs after repeated protein additions as well as to discard samples with unevenly distributed eGFP-His_6 within the chamber or samples in which the lipid concentration varies over the measuring time (i.e. due to GUVs burst). Moreover, the lipid dynamics of each GUV can be probed simultaneously, thus adding a further control point.

Finally, one should consider the actual measurement time of each of these assays. In order to be able to precisely measure the average number of particles as well as the diffusion time in the GUV–FCS approach, it is necessary to collect data over a time period of several minutes. Thus, the time for an experiment easily sums up when averaging several GUVs per protein concentration. On the other hand, in both GUV-imaging and LUV–FCS assays the actual measurement time reduces to less than 2 h, while having approximately the same work load for calibration and data treatment (Table 2).

5. Conclusions

The partition coefficient K_P is a very useful parameter to compare the affinity of anchoring segments of peripheral proteins for membranes of different lipid compositions. Despite the variety of methods known for determining K_P, all of them possess drawbacks that could affect their accuracy. We provide a new, complementary and versatile method to determine K_Ps, which is useful in experimental situations where other methods are not feasible and allows to directly measure membrane affinities of protein systems reconstituted in GUVs. Moreover we showed how to understand the relation between K_P and the number of molecules per lipid surface (Eq. (8)), which can always be determined for a lipid–protein system, whose soluble protein and lipid surface concentrations are known. To our knowledge, this is the first assay based on GUVs, which combines confocal imaging with FCS to precisely determine protein concentrations at equilibrium. Small amounts of sample are needed, since the measurement can be conducted in low volume chambers and FCS as well as photon-counting imaging are known to be sensitive down to the nanomolar range. In addition, our assay accounts for loss of protein, due for example to unspecific interactions with the chamber or pipetting errors, since free and membrane associated protein are always directly determined. Moreover, the use of free standing membranes excludes any effects of the support on protein–lipid interaction. Apart from studying the interaction of peripheral proteins with lipid membranes, any fluorescent species, e.g. labeled peptides or small molecules, could be investigated with this assay. In particular, we measured the K_P of the peptide corresponding to the effector domain of the MARCKS protein using the GUV–FCS approach, and found our results to be in line with the published data using LUVs.

The comparison of our results with a FCS based LUV assay revealed that the later method is not accurate for the NTA(Ni)-His_6 system, even when taking into account the multiple binding of peptides to a single vesicle. Due to vesicle aggregation, no significant increase of the partition coefficient was detected (one-way ANOVA, $F(3,14) = 3.3$, $p = 0.061$) even in the presence of 2.5 times the amount of binding sides in the membrane. The K_Ps obtained with our dual approach show a dependence on the content of NTA(Ni) lipids in the membrane, and serve as a reference for future work employing this membrane anchoring strategy for reconstituting protein systems in GUVs.

Finally, our imaging-based GUV assay could be readily combined with an automated GUV analysis software [56] or performed in a microarray setup [57] to directly extract the mean intensities of several GUVs in one image or simultaneously probe different lipid binding proteins in a single experiment, while significantly reducing both measuring and analysis time.

Table 2
Comparison of the methods.

	GUV–FCS	GUV-imaging	LUV–FCS
Measurement time per sample	5 h	2 h	2 h
Accuracy/precision	High/low[a]	High/high	Low[b]/high
Accessible lipid concentration (M)	10^{-9}–10^{-6}	10^{-9}–10^{-6}	10^{-6}–10^{-3} [15]
Protein concentration (M)	10^{-9}–10^{-6}	10^{-8}–10^{-4}	10^{-9}–10^{-6} [15]

[a] If the free protein concentration is calculated only once.
[b] For protein-induced vesicle aggregation.

Author information

The authors declare no competing financial interest.

Acknowledgments

We thank Dr. Henri G. Franquelim for fruitful discussions, Stefan Pettera and Dr. Stephan Uebel of the MPI-B core facility for synthesizing and labeling the MARCKS peptide, respectively.

Appendix A. Supplementary information

Supplementary information to this article can be found online at http://dx.doi.org/10.1016/j.bbamem.2015.09.001.

References

[1] W. Cho, R.V. Stahelin, Membrane–protein interactions in cell signaling and membrane trafficking, Annu. Rev. Biophys. Biomol. Struct. 34 (2005) 119–151.
[2] S. Munro, Organelle identity and the targeting of peripheral membrane proteins, Curr. Opin. Cell Biol. 14 (2002) 506–514.
[3] R.V. Stahelin, Lipid binding domains: more than simple lipid effectors, J. Lipid Res. 50 (2008) S299–S304.
[4] J. Murphy, K. Knutson, A. Hinderliter, Protein–lipid interactions: role of membrane plasticity and lipid specificity on peripheral protein interactions, Methods Enzymol. 466 (2009) 431–453.
[5] A.L. Lomize, I.D. Pogozheva, M.A. Lomize, H.I. Mosberg, The role of hydrophobic interactions in positioning of peripheral proteins in membranes, BMC Struct. Biol. 7 (2007) 44.
[6] A. Mulgrew-Nesbitt, K. Diraviyam, J. Wang, S. Singh, P. Murray, Z. Li, L. Rogers, N. Mirkovic, D. Murray, The role of electrostatics in protein–membrane interactions, Biochim. Biophys. Acta 1761 (2006) 812–826.
[7] S.H. White, W.C. Wimley, A.S. Ladokhin, K. Hristova, Protein folding in membranes: determining energetics of peptide–bilayer interactions, Methods Enzymol. 295 (1998) 62–87.
[8] W. Cho, L. Bittova, R.V. Stahelin, Membrane binding assays for peripheral proteins, Anal. Biochem. 296 (2001) 153–161.
[9] H. Zhao, P. Lappalainen, A simple guide to biochemical approaches for analyzing protein–lipid interactions, Mol. Biol. Cell 23 (2012) 2823–2830.
[10] J.L. Scott, C.A. Musselman, E. Adu-Gyamfi, T.G. Kutateladze, R.V. Stahelin, Emerging methodologies to investigate lipid–protein interactions, Integr. Biol. 4 (2012) 247–258.
[11] N.C. Santos, M. Prieto, M.A.R.B. Castanho, Quantifying molecular partition into model systems of biomembranes: an emphasis on optical spectroscopic methods, Biochim. Biophys. Acta 1612 (2003) 123–135.
[12] M. Kang, C.A. Day, E. DiBenedetto, A.K. Kenworthy, A quantitative approach to analyze binding diffusion kinetics by confocal FRAP, Biophys. J. 99 (2010) 2737–2747.
[13] C.B. Fox, J.R. Wayment, G.A. Myers, S.K. Endicott, J.M. Harris, Single-molecule fluorescence imaging of peptide binding to supported lipid bilayers, Anal. Chem. 81 (2009) 5130–5138.
[14] N.S. Hatzakis, V.K. Bhatia, J. Larsen, K.L. Madsen, P.-Y. Bolinger, A.H. Kunding, J. Castillo, U. Gether, P. Hedegård, D. Stamou, How curved membranes recruit amphipathic helices and protein anchoring motifs, Nat. Chem. Biol. 5 (2009) 835–841.
[15] L. Rusu, A. Gambhir, S. McLaughlin, J. Rädler, Fluorescence correlation spectroscopy studies of peptide and protein binding to phospholipid vesicles, Biophys. J. 87 (2004) 1044–1053.
[16] A. Horner, F. Goetz, R. Tampé, E. Klussmann, P. Pohl, Mechanism for targeting the A-kinase anchoring protein AKAP18δ to the membrane, J. Biol. Chem. 287 (2012) 42495–42501.
[17] G. Blin, E. Margeat, K. Carvalho, C.A. Royer, C. Roy, C. Picart, Quantitative analysis of the binding of ezrin to large unilamellar vesicles containing phosphatidylinositol 4,5 bisphosphate, Biophys. J. 94 (2008) 1021–1033.
[18] E. Rhoades, T.F. Ramlall, W.W. Webb, D. Eliezer, Quantification of α-synuclein binding to lipid vesicles using fluorescence correlation spectroscopy, Biophys. J. 90 (2006) 4692–4700.

[19] Y.O. Posokhov, M.V. Rodnin, L. Lu, A.S. Ladokhin, Membrane insertion pathway of annexin B12: thermodynamic and kinetic characterization by fluorescence correlation spectroscopy and fluorescence quenching, Biochemistry 47 (2008) 5078–5087.
[20] B. Wu, Y. Chen, J.D. Mueller, Fluorescence correlation spectroscopy of finite-sized particles, Biophys. J. 94 (2008) 2800–2808.
[21] H. Engelke, I. Dorn, J.O. Raedler, Diffusion and molecular binding in crowded vesicle solutions measured by fluorescence correlation spectroscopy, Soft Matter 5 (2009) 4283–4289.
[22] A.M. Melo, M. Prieto, A. Coutinho, The effect of variable liposome brightness on quantifying lipid–protein interactions using fluorescence correlation spectroscopy, Biochim. Biophys. Acta Biomembr. (2011) 1–10.
[23] V. Betaneli, P. Schwille, Fluorescence correlation spectroscopy to examine protein–lipid interactions in membranes, Methods Mol. Biol. 974 (2013) 253–278.
[24] A.J. García-Sáez, P. Schwille, Fluorescence correlation spectroscopy for the study of membrane dynamics and protein/lipid interactions, Methods 46 (2008) 116–122.
[25] S. Chiantia, J. Ries, P. Schwille, Fluorescence correlation spectroscopy in membrane structure elucidation, Biochim. Biophys. Acta 1788 (2009) 225–233.
[26] P. Walde, K. Cosentino, H. Engel, P. Stano, Giant vesicles: preparations and applications, Chem. Eur. J. of Chem. Bio. 11 (2010) 848–865.
[27] S. Knecht, D. Ricklin, A.N. Eberle, B. Ernst, Oligohis-tags: mechanisms of binding to Ni^{2+}-NTA surfaces, J. Mol. Recognit. 22 (2009) 270–279.
[28] F. Khan, M. He, M.J. Taussig, Double-hexahistidine tag with high-affinity binding for protein immobilization, purification, and detection on Ni-nitrilotriacetic acid surfaces, Anal. Chem. 78 (2006) 3072–3079.
[29] I. López-Montero, P. López-Navajas, J. Mingorance, M. Vélez, M. Vicente, F. Monroy, Membrane reconstitution of FtsZ–ZipA complex inside giant spherical vesicles made of *E. coli* lipids: large membrane dilation and analysis of membrane plasticity, Biochim. Biophys. Acta Biomembr. 1828 (2013) 687–698.
[30] W. Römer, L.-L. Pontani, B. Sorre, C. Rentero, L. Berland, V. Chambon, C. Lamaze, P. Bassereau, C. Sykes, K. Gaus, L. Johannes, Actin dynamics drive membrane reorganization and scission in clathrin-independent endocytosis, Cell 140 (2010) 540–553.
[31] A.J. García-Sáez, J. Ries, M. Orzáez, E. Pérez-Payà, P. Schwille, Membrane promotes tBID interaction with BCL(XL), Nat. Struct. Mol. Biol. 16 (2009) 1178–1185.
[32] J.C. Stachowiak, E.M. Schmid, C.J. Ryan, H.S. Ann, D.Y. Sasaki, M.B. Sherman, et al., Membrane bending by protein–protein crowding, Nat. Cell Biol. 14 (2012) 944–949.
[33] A. Arbuzova, L. Wang, J. Wang, G. Hangyás-Mihályné, D. Murray, B. Honig, S. McLaughlin, Membrane binding of peptides containing both basic and aromatic residues. Experimental studies with peptides corresponding to the scaffolding region of caveolin and the effector region of MARCKS, Biochemistry 39 (2000) 10330–10339.
[34] T. Weidemann, M. Wachsmuth, T.A. Knoch, G. Muller, W. Waldeck, J. Langowski, Counting nucleosomes in living cells with a combination of fluorescence correlation spectroscopy and confocal imaging, J. Mol. Biol. 334 (2003) 229–240.
[35] M.I. Angelova, D.S. Dimitrov, Liposome electroformation, Faraday Discuss. 81 (1986) 303–311.
[36] G. Rouser, S. Fkeischer, A. Yamamoto, Two dimensional then layer chromatographic separation of polar lipids and determination of phospholipids by phosphorus analysis of spots, Lipids 5 (1970) 494–496.
[37] E.R. Middleton, E. Rhoades, Effects of curvature and composition on α-synuclein binding to lipid vesicles, Biophys. J. 99 (2010) 2279–2288.
[38] F. Heinemann, V. Betaneli, F.A. Thomas, P. Schwille, Quantifying lipid diffusion by fluorescence correlation spectroscopy: a critical treatise, Langmuir 28 (2012) 13395–13404.
[39] Z. Petrášek, P. Schwille, Precise measurement of diffusion coefficients using scanning fluorescence correlation spectroscopy, Biophys. J. 94 (2008) 1437–1448.
[40] T. Dertinger, V. Pacheco, I. von der Hocht, R. Hartmann, I. Gregor, J. Enderlein, Two-focus fluorescence correlation spectroscopy: a new tool for accurate and absolute diffusion measurements, ChemPhysChem 8 (2007) 433–443.
[41] P. Müller, P. Schwille, T. Weidemann, PyCorrFit-generic data evaluation for fluorescence correlation spectroscopy, Bioinformatics 30 (2014) 2532–2533.
[42] S. Rüttinger, V. Buschmann, B. Krämer, R. Erdmann, R. Macdonald, F. Koberling, Comparison and accuracy of methods to determine the confocal volume for quantitative fluorescence correlation spectroscopy, J. Microsc. 232 (2008) 343–352.
[43] E.P. Petrov, P. Schwille, State of the art and novel trends in fluorescence correlation spectroscopy, in: U. Resch-Genger (Ed.), Standardization and Quality Assurance in Fluorescence Measurements II, Springer Berlin Heidelberg 2008, pp. 145–197.
[44] F.A. Thomas, I. Visco, Z. Petrášek, F. Heinemann, P. Schwille, Diffusion coefficients and dissociation constants of enhanced green fluorescent protein anchored to free standing membranes, Data in Brief Submitted.
[45] C.A. López, A.H. de Vries, S.J. Marrink, Computational microscopy of cyclodextrin mediated cholesterol extraction from lipid model membranes, Sci. Rep. 3 (2013) 2071.
[46] J. Larsen, N.S. Hatzakis, D. Stamou, Observation of inhomogeneity in the lipid composition of individual nanoscale liposomes, J. Am. Chem. Soc. 133 (2011) 10685–10687.
[47] J. Pan, S. Tristram-Nagle, N. Kučerka, J.F. Nagle, Temperature dependence of structure, bending rigidity, and bilayer interactions of dioleoylphosphatidylcholine bilayers, Biophys. J. 94 (2008) 117–124.
[48] K.J. Oh, S. Barbuto, K. Pitter, J. Morash, L.D. Walensky, S.J. Korsmeyer, A membrane-targeted BID BCL-2 homology 3 peptide is sufficient for high potency activation of BAX in vitro, J. Biol. Chem. 281 (2006) 36999–37008.
[49] J. Enderlein, T. Ruckstuhl, S. Seeger, Highly efficient optical detection of surface-generated fluorescence, Appl. Opt. 38 (1999) 724–732.
[50] J. Ries, E.P. Petrov, P. Schwille, Total internal reflection fluorescence correlation spectroscopy: effects of lateral diffusion and surface-generated fluorescence, Biophys. J. 95 (2008) 390–399.
[51] N. Kučerka, S. Tristram-Nagle, J.F. Nagle, Structure of fully hydrated fluid phase lipid bilayers with monounsaturated chains, J. Membr. Biol. 208 (2005) 193–202.
[52] J. Pan, X. Cheng, L. Monticelli, F.A. Heberle, N. Kučerka, D.P. Tieleman, J. Katsaras, The molecular structure of a phosphatidylserine bilayer determined by scattering and molecular dynamics simulations, Soft Matter 10 (2014) 3716–3725.
[53] J.D. Patel, R. O'Carra, J. Jones, J.G. Woodward, R.J. Mumper, Preparation and characterization of nickel nanoparticles for binding to his-tag proteins and antigens, Pharm. Res. 24 (2007) 343–352.
[54] A.N. Kapanidis, Y.W. Ebright, R.H. Ebright, Site-specific incorporation of fluorescent probes into protein: hexahistidine-tag-mediated fluorescent labeling with $(Ni^{2+}$: nitrilotriacetic acid$)_n$-fluorochrome conjugates, J. Am. Chem. Soc. 123 (2001) 12123–12125.
[55] G.G. Chikh, W.M. Li, M.-P. Schutze-Redelmeier, J.-C. Meunier, M.B. Bally, Attaching histidine-tagged peptides and proteins to lipid-based carriers through use of metal-ion-chelating lipids, Biochim. Biophys. Acta 1567 (2002) 204–212.
[56] E. Hermann, S. Bleicken, Y. Subburaj, A.J. García-Sáez, Automated analysis of giant unilamellar vesicles using circular Hough transformation, Bioinformatics 30 (2014) 1747–1754.
[57] A.-E. Saliba, I. Vonkova, S. Ceschia, G.M. Findlay, K. Maeda, C. Tischer, S. Deghou, V. van Noort, P. Bork, T. Pawson, J. Ellenberg, A.-C. Gavin, A quantitative liposome microarray to systematically characterize protein–lipid interactions, Nat. Methods 11 (2014) 47–50.